International Journal of Biological Macromolecules 357 (2026) 151585

Contents lists available at ScienceDirect

International Journal of Biological Macromolecules

journal homepage: www.elsevier.com/locate/ijbiomac

Unraveling the NMR structures of G-quadruplex-forming aptamers acting as inhibitors of High Mobility Group Box 1 (HMGB1) pathological activity

Marko Trajkovski [a,1], Chiara Platella [b,1], Domenica Musumeci [b,c,1], Ettore Napolitano [b], Carla Lucia Esposito [d], Silvia Catuogno [d], Janez Plavec [a,*], Daniela Montesarchio [b,*]

[a] Slovenian NMR Centre, National Institute of Chemistry, Hajdrihova 19, SI-1000, Ljubljana, Slovenia
[b] Department of Chemical Sciences, University of Naples Federico II, via Cintia 21, I-80126, Naples, Italy
[c] Institute of Biostructure and Bioimaging (IBB), National Research Council (CNR), I-80145, Naples, Italy
[d] Institute of Endotypes in Oncology, Metabolism and Immunology "G. Salvatore" (IEOMI), National Research Council (CNR), via Sergio Pansini 5, I-80131, Naples, Italy

ARTICLE INFO

Keywords:
Anti-HMGB1 aptamers
G-quadruplex
NMR structure

ABSTRACT

High Mobility Group Box 1 (HMGB1) is a valuable therapeutic target in inflammatory, autoimmune diseases, and cancer. Recently, some of us identified a set of anti-HMGB1 aptamers, folding into G-quadruplex structures of different topology. Among them, L12 and L41 were the most effective aptamers as for affinity and activity towards the protein.

Here, nuclear magnetic resonance (NMR) spectroscopy, corroborated by size exclusion high performance liquid chromatography (SE-HPLC) and circular dichroism (CD), allowed defining the structural features of L12 and L41. In-depth structural details were obtained for the monomeric forms of these aptamers in a K^+-rich (100 mM K^+) buffer, mimicking the intracellular environment. Under these conditions, both L12 and L41 folded in hybrid G-quadruplex structures. By cross-referencing the obtained data, we inferred that these structures were also the main monomeric folded species in the Na^+-rich Phosphate Buffered Saline (PBS) buffer, mimicking the extracellular environment, suggesting that these aptamers share similar recognition patterns when interacting with the target protein. However, in PBS a higher amount of hybrid-2 G-quadruplex was observed for L12 than L41. Biolayer interferometry (BLI) analysis demonstrated a preference of HMGB1 for L12 over L41, in line with *in vitro* assays, showing higher ability to inhibit the HMGB1-induced cell migration for L12 than L41. These findings suggest that HMGB1 recognizes the hybrid-2 G-quadruplex folding of these aptamers, present in higher degree in L12 than L41. In summary, this work provides precious insights into the conformational preferences of L12 and L41, of crucial importance to design more effective HMGB1 inhibitors.

1. Introduction

The highly conserved non-histone DNA-binding protein HMGB1 (High Mobility Group Box 1) is essential for several vital cellular processes, such as regulation of gene transcription, DNA remodelling and repair [1]. As a DNA chaperone, this protein is well-known for its high affinity towards various non-canonical DNA structures, such as bent duplexes, cisplatin-modified or UV-damaged duplexes, as well as four-way junctions or G-quadruplexes [2–5]. When released in the extracellular matrix, HMGB1 can act as a cytokine, thus playing an essential role in immune and inflammatory response [6]. Furthermore, HMGB1 has a crucial role in the pathogenesis of a plethora of diseases, such as cancer, neurodegeneration and inflammation [7,8]. In cancer, HMGB1 is involved in multiple important processes that promote tumour growth, progression and metastasis. Moreover, it can induce angiogenesis by promoting the release of pro-inflammatory cytokines and growth factors [9]. Therefore, targeting HMGB1 and inhibiting its signalling activity may be a valuable therapeutic approach for the treatment of inflammation and cancer.

By an *in vitro* selection process starting from a focused library of guanine-rich oligonucleotides, some of us recently discovered a series of G-quadruplex-forming aptamers able to efficiently recognize HMGB1 and inhibit cancer cell migration induced by the protein [4]. Using spectroscopic, electrophoretic and chromatographic methods, the

* Corresponding authors.
E-mail addresses: janez.plavec@ki.si (J. Plavec), daniela.montesarchio@unina.it (D. Montesarchio).
[1] These authors equally contributed to this work.

https://doi.org/10.1016/j.ijbiomac.2026.151585
Received 30 December 2025; Received in revised form 19 March 2026; Accepted 20 March 2026
Available online 24 March 2026

identified aptamers were investigated in PBS (phosphate buffer saline), a buffer mimicking the extracellular environment where HMGB1 displays pathogenic activity. Under these conditions, the oligonucleotides proved to fold into unimolecular G-quadruplexes of different topology, with the most bioactive ones also spontaneously forming very stable dimeric and/or higher-order G-quadruplex structures.

Among the examined oligonucleotides, L12 and L41, of sequence 5′-d(TTA-GGG-ATT-GGG-AAT-GGG-TAT-GGG-TT)-3′ and 5′-d(TTA-GGG-AAA-GGG-TAT-GGG-AAA-GGG-TT)-3′, respectively, emerged as very promising HMGB1 inhibitors, being endowed with strong affinity towards the protein and excellent ability to block HMGB1-induced cell migration. L12 and L41 also showed optimal features as potential candidate drugs, both folded into G-quadruplex structures having remarkable thermal stability and enzymatic resistance. Interestingly, these aptamers were able to fold in both monomeric and dimeric/higher-order G-quadruplex structures, present in PBS at a ratio of *ca.* 40:60 for L12 or 30:70 for L41. In the case of L12, the dimeric/higher-order species were isolated, showing to be very stable after separation, not interconverting over time, and exhibiting affinity for HMGB1 in the nanomolar range [4].

Stimulated by the promising biological activity of L12 and L41, we decided to investigate their three-dimensional structures so to undertake a program of rational design and synthesis of optimized anti-HMGB1 aptamers. Aiming at elucidating the structural features of L12 and L41, we have here analyzed both the monomeric and higher-order species of these aptamers by NMR spectroscopy. In-depth structural details were obtained by NMR in a K^+-rich (100 mM K^+) buffer for the monomeric forms of both the aptamers. By cross-referencing the NMR data with those obtained from circular dichroism (CD) and size exclusion high performance liquid chromatography (SE-HPLC) analyses, we inferred that the characterized structures were also the main monomeric folded species in PBS. The monomeric L12 and L41 aptamers were further analyzed in their interaction with HMGB1 in PBS by CD and biolayer interferometry (BLI) and finally tested for their anti-HMGB1 activity in cell assays, thus correlating their conformational features with their ability to bind and inhibit the target protein.

2. Materials and methods

2.1. DNA synthesis and purification

Oligonucleotides named L12 and L41, corresponding to the sequences 5′-d(TTA-GGG-ATT-GGG-AAT-GGG-TAT-GGG-TT)-3′ and 5′-d(TTA-GGG-AAA-GGG-TAT-GGG-AAA-GGG-TT)-3′ respectively, were synthesized on DNA/RNA H-8 Synthesizer (K&A Laborgeräte GbR) by standard phosphoramidite chemistry according to DMT-ON mode, *i.e.* retaining the final 4,4′-dimethoxytrityl (DMT) protecting group. Analogously, a series of L12 oligonucleotides differing for the position of partially ^{13}C- and ^{15}N-isotope labelled guanines or thymines were also prepared using the proper labelled phosphoramidites. After the synthesis, cleavage of the oligonucleotides from the solid support along with phosphates and nucleobases deprotection were achieved upon incubation with AMA solution (1:1 mixture of aqueous 30% ammonium hydroxide and 40% aqueous methylamine) at 65 °C for 30 min. The samples were purified and DMT removed by using Glen-Pak cartridges (Glen Research) following the manufacturer's protocol. After purification, the solvent was evaporated and the samples were dissolved in 500 mM LiCl and then fully desalted by exhaustive washings with Milli-Q water by using Amicon® ultrafiltration devices with 3 KDa molecular weight cut off (MWCO), until obtaining the stock desalted solution of DNA in pure water, comprising less than 0.05 mM LiCl at pH between 5 and 6. The concentrations of DNA oligonucleotide in stock solutions were determined by analyzing UV absorption at 260 nm (molar extinction coefficients at this wavelength were obtained by the Oligo Calculator program at the website: https://oligocalc.eu/). Vivaspin® Turbo 4 ultrafiltration units with 10 KDa MWCO (Sartorius AG) were used and several filtration steps at 1000 g for 10 min were performed (fixed-angle rotor) to separate the monomeric and dimeric/higher-order species of L12 and L41 dissolved in PBS (137 mM NaCl, 2.7 mM KCl, 10 mM Na_2HPO_4, 1.8 mM KH_2PO_4, pH 7.3). The purity and molecularity of the separated species were checked by SE-HPLC adopting previously reported protocols [4] as also described in Subsection 2.3.

2.2. NMR studies

2.2.1. NMR samples

NMR samples were prepared by diluting the desalted stock solutions of DNA oligonucleotides in pure water at 90%/10% $H_2O/^2H_2O$, including or not 20 mM potassium phosphate (KPi) buffer (pH 7.0) or 20 mM sodium phosphate (NaPi) buffer (pH 7.0). The final oligonucleotide concentrations in NMR samples were in the range between 0.2 and 1.0 mM per DNA strand. The NMR samples were titrated with increasing concentrations of KCl and NaCl in the range between 10 and 200 mM. In addition, NMR samples of monomeric and dimeric/higher-order species of L12 and L41 in PBS isolated after separation by ultrafiltration, as described in subsection 2.1, were used for NMR experiments after addition of 90%/10% $H_2O/^2H_2O$ so to obtain a final oligonucleotide concentration of 0.2 mM.

2.2.2. NMR analysis

NMR data were collected on Bruker AVANCE NEO 600 and 800 MHz NMR spectrometers equipped with cryogenic probes. The 1D NMR experiments were performed at temperatures in the range between 5 and 37 °C and 2D NMR experiments were performed at 25 °C, if not stated otherwise. Suppression of water signal in NMR spectra was achieved by using excitation sculpting method. NMR spectra were externally referenced to sodium trimethylsilylpropanesulfonate (DSS). NMR spectra were processed and analyzed using TopSpin (Bruker) software and NMRFAM-SPARKY [10].

2.2.3. Structural restraints and calculations

Starting structures were generated with the use of leap module of AMBER 22 and 3DNA software packages [11,12]. The distance restraints used in L12 and L41 structural calculations were derived from the integral values of cross-peaks in 2D ^1H–^1H NOESY acquired at mixing time (τm) 120 and 200 ms, respectively. The integral values were determined in NMRFAM-SPARKY using Gaussian line-shape fitting. The average volume of H1'-H8 for cross-peaks from adenine and guanine residues exhibiting glycosidic bond torsion angle (χ) in *anti* conformation was used as a reference distance of 3.9 Å. Restraints were subsequently classified into three categories: strong (1.8–3.6 Å), medium (2.6–5.0 Å), and weak (3.5–6.5 Å).

The calculations included restrained 1000 ps long simulated annealing (SA) protocol. The force constants were 5 kcal mol^{-1} $Å^{-2}$ for NOE-based distance, hydrogen-bond and planarity of guanine residues in quartets, while 100 kcal mol^{-1} rad^{-2} for chirality restraints. The force constants for glycosidic bond angles were 20 kcal mol^{-1} rad^{-2} when calculating L12 structures, while they were 200 kcal mol^{-1} rad^{-2} when calculating L41 structures, thereby to overcome the local steric barriers during the simulated annealing protocol and ensure that the calculated structures converged to the experimentally validated A19 *syn* conformation in L41 G-quadruplex. The scalar factor for the force constants for restraints was held constant at the initial value of 0.1 for the first 50 ps, scaled to the final value of 1.0 between 50 and 500 ps and then held constant until the end of the calculation. Notably, the protocol for the scalar factor for restraint force constants was designed to facilitate broad sampling of the conformational landscape and prevent kinetic trapping during the early stages of simulated annealing. The protocols included heating over the first 50 ps from 0 to 1000 K, followed by 150 ps equilibration at 1000 K, cooling over 700 ps from 298 to 0 K and additional 100 ps at 0 K. Hundred structures were calculated and ten structures with the lowest energy were minimized and selected as the

final ensemble used for structural analysis.

2.3. SE-HPLC analysis

SE-HPLC analysis of the oligonucleotide samples in the buffer and at the concentration indicated was performed on an Agilent HPLC system, equipped with a UV/vis detector, and a Yarra 3 μm analytical column (300 × 4.60 mm; Phenomenex). The elution was monitored at λ = 254 nm using a 0.35 mL min^{-1} flow rate. PBS, 20 mM NaPi/100 mM NaCl or 20 mM KPi/100 mM KCl buffers (pH 6.9), were used as the mobile phases as specified, and volumes of each oligonucleotide solutions corresponding to *ca.* 0.2 nmol were loaded at each injection. Injections of each sample were performed in triplicate. The error associated with the retention time (t_R) determination is within ±5%.

2.4. CD analysis

CD spectra were recorded on a Jasco J-1500 spectropolarimeter equipped with a Jasco CTU-100 circulating thermostat unit. The experiments were performed by using a quartz cuvette with a path length of 1 cm or a two-chamber quartz cell (2 × 0.4375 cm optical pathlength and 2 × 1 mL internal volume). The spectra were recorded in the 200–320 nm range with 5 accumulations, 100 nm/min scanning speed, 4 s response and 2.0 nm bandwidth and were corrected by subtraction of the background scan with buffer. For the CD-monitored titration experiments, CD spectra were recorded: i) on the oligonucleotide samples at 2 μM concentration in water – prepared by dilution from their concentrated stock solutions – and after adding, first, ii) 20 mM of the proper phosphate buffer (sodium or potassium) and then iii) increasing concentrations of NaCl or KCl (from 10 to 100 mM). For the CD-melting experiments, the ellipticity was recorded with a temperature scan rate of 1 °C/min. In addition, during the temperature ramp, CD spectra of the sample were recorded every 5 °C. Generally, the selected wavelength for monitoring the unfolding processes corresponded to the maximum CD signal of characteristic bands (*i.e.*, *ca.* 290, 295 and 260 nm for hybrid, antiparallel and parallel G-quadruplex, respectively, as described in detail in Section 3). As far as the experiments with the two-chamber quartz cell are concerned, the oligonucleotides and the protein were placed in the two separate chambers of the cell at a concentration of 2 μM each in PBS buffer to record the *sum* spectra. Then, the cuvette was turned upside down, allowing the content of the two adjacent chambers to mix and form a homogeneous solution distributed in both parts of the cell, and the *mix* spectra were recorded. Spectra of each oligonucleotide and protein alone were also recorded as references, filling one of the two chambers with 2 μM solutions of L12, L41 or protein in PBS buffer. CD spectra for each sample as well as CD-melting and CD-binding experiments were performed at least in duplicate on independent sample solutions, always showing consistent data. T_m values were estimated as the minima of the first derivative plots of the melting curves and the error associated with the T_m determination was ±1 °C.

2.5. BLI binding studies

BLI analysis was performed on an Octet R2 system (Sartorius). L12 and L41 carrying a biotin tag at their 5′-end were purchased from Biomers.net GmbH (Germany) as HPLC-purified and desalted DNA oligomers in lyophilized form. All steps were performed at 20 °C by shaking at 1000 rpm in a 96-well plate containing 200 μL of different samples in the binding buffer, *i.e.* PBS, BSA (0.1%, *w/v*), Tween-20 (0.02%, *v*/v), pH 7.4, in each well. For the regeneration steps, a buffer having the same composition as the binding buffer and supplemented with 0.001% SDS was added to the wells. The biotinylated oligonucleotides, dissolved at 50 nM concentration in PBS, were immobilized on the streptavidin-coated sensors (Octet SA Biosensors, Sartorius). The method used to functionalize the sensors included the following steps: baseline (1 min); loading (2 min); baseline (1 min); regeneration (5 s for three times), baseline 2 (3 min). The HMGB1 protein was then added at various concentrations in the different wells, which were analyzed for an association time of 3 min and a dissociation time of 5 min. In detail, 125, 250, 500 and 1000 nM HMGB1 concentrations were used for both L12 for L41. The protein solutions and blank samples containing only the reference binding buffer were analyzed in parallel by two different functionalized sensors. Normalization of the sensorgrams relative to the oligonucleotides-HMGB1 interaction was carried out by subtracting the signal simultaneously acquired from the reference functionalized sensor, so to eliminate the buffer-induced interferometry shift contribution using Octet Analysis Studio Version 13.0.3.52. A 1:1 fitting model was used [13]. Experiments were carried out in duplicate and data were reported as average values ± SD (standard deviation).

2.6. In vitro cell migration assay

A549 NSCLC (non-small-cell lung cancer) cells (ATCC) were cultured in RPMI medium supplemented with 1% penicillin/streptomycin solution (Sigma-Aldrich) and 10% FBS (Sigma-Aldrich). For the migration assay, cells were seeded in 12 well plates (75000 cells/well) and left untreated or treated with 100 nM of monomeric L12 and L41, or of scr, unable to form G-quadruplex structures and thus used as negative control. After 24 h, cells were detached, washed in serum-free medium, counted and 50000 cells/point in 0.1 mL were seeded in the upper chamber of a transwell (8 μM pore size) in the absence or presence of the corresponding oligonucleotide (100 nM). 600 μL of 10% complete medium were added in the lower chamber as chemoattractant. After 24 h, migrated cells were stained with 1% Crystal Violet (25% methanol solution) and photographed under the phase-contrast microscope at 10× magnification. For quantitative analysis, Crystal Violet was eluted with 1% SDS and quantified at a microplate reader (Thermofisher) by measuring the absorbance at 590 nm. The scr oligonucleotide, corresponding to the nucleotide sequence 5′-d(AAGTGT GTGTGTGTGTGTGTGAAG)-3′, was purchased from Biomers.net GmbH (Germany) as HPLC-purified and desalted DNA oligomer and obtained in lyophilized form. Three independent biological replicates (*n* = 3) were performed; in the single experiment, each point was taken in triplicate. Reported data represent the mean ± SD of the three independent experiments. Statistical analysis was performed by one-way ANOVA with Turkey's multiple comparison using GraphPad Prism.

3. Results and discussion

3.1. NMR characterization and SE-HPLC/CD analyses of the anti-HMGB1 aptamers L12 and L41

The anti-HMGB1 aptamers L12 and L41 have been recently characterized by spectroscopic, electrophoretic and chromatographic techniques in the PBS buffer (137 mM NaCl, 2.7 mM KCl, 10 mM Na_2HPO_4, 1.8 mM KH_2PO_4, pH 7.3) which mimics the extracellular medium where HMGB1 exerts its pathogenic activity [4]. In these conditions, both L12 and L41 fold in monomeric and dimeric/higher-order G-quadruplex structures which can be separated and individually analyzed (see Materials and Methods for details).

Unfortunately, the ^{1}H NMR spectra of the monomeric and dimeric/higher-order species of both L12 and L41 in PBS buffer showed low resolution or a broad hump in the imino region (δ 10.4–12.2 ppm) characteristic of G-quadruplex structures (Fig. 1), preventing a deeper NMR characterization of the two aptamers in this buffer. Considering that PBS buffer contains both sodium and potassium ions, different buffers containing only Na^+ or only K^+ were explored to allow an in-depth NMR characterization of the aptamers under different solution conditions. However, for the dimeric/higher-order species of L12 and L41, no improvement in the resolution of the ^{1}H NMR spectra was obtained not allowing the structural characterization of these species. Therefore, we focused on the NMR analysis of the monomeric forms of

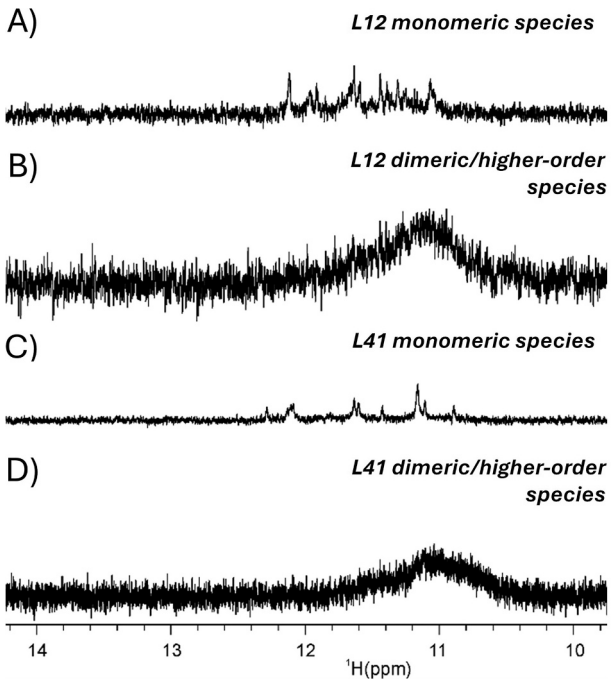

Fig. 1. Imino regions of ^{1}H NMR spectra of: A) monomeric L12; B) dimeric/higher-order species of L12; C) monomeric L41 and D) dimeric/higher-order species of L41, all dissolved in PBS buffer. The spectra were recorded on an 800 MHz NMR spectrometer at 25 °C, in 90%/10% $H_2O/^2H_2O$ at 0.2 mM (A and C) and 0.1 mM (B and D) concentration per strand.

L12 and L41 for which high-resolution structures could be obtained.

3.1.1. *Studies of L12 aptamer in Na^+-containing buffer*

The ^{1}H NMR spectrum of desalted L12 dissolved in pure water at 25 °C exhibited broad imino signals between δ ^{1}H 10.7 and 11.0 ppm (Fig. 2A) which, together with the number of mostly well-resolved signals in the aromatic spectral region, suggested absence of a well-defined structure. In comparison, in the presence of 20 mM sodium phosphate (NaPi) buffer, ^{1}H NMR spectrum of L12 exhibited very weak (at the level of detection) ^{1}H NMR imino signals, dispersed across a notably larger chemical shift range, *i.e.* between δ ^{1}H 10.4 and 11.9 ppm (Fig. 2B), indicative of formation of a discrete G-quadruplex structure, which however corresponded to a minor species. The twelve imino resonances diagnostic of the G-quadruplex structure gave more intense signals upon addition of increasing amounts of NaCl (from 10 to 100 mM, Fig. 2C-E), consistent with Na^+ ions promoting the formation of a well-defined structure exhibiting three G-quartets. Notably, even at 100 mM NaCl this G-quadruplex structure accounted for only around 20–30% of L12.

Upon heating L12 from 25 to 37 °C in the presence of 100 mM NaCl (Fig. S1A–B), the NMR signals for the G-quadruplex broadened significantly, nearly to the baseline. This observation is consistent with a temperature-driven depletion of the minor G-quadruplex species in favour of the unfolded DNA, suggesting a relatively low thermal stability of L12 G-quadruplex in the sole presence of Na^+ ions (*vide infra*). By comparing these results with the ^{1}H NMR spectrum of L12 in the absence of NaCl at 25 °C (Fig. S1C), which exhibits only the signals of the unfolded state, we were able to trace and assign the corresponding signals of this form in the spectrum of L12 in the solution comprising 100 mM NaCl acquired at 37 °C.

Moreover, almost a perfect match between the ^{1}H NMR spectra of L12 acquired at 0.2 and 1.0 mM oligonucleotide concentrations (Fig. S2) was observed, suggesting intramolecular topology of the G-quadruplex structure in the presence of Na^+ ions.

In the attempt to unambiguously assign ^{1}H NMR chemical shifts, a series of L12 oligonucleotides differing by position of partially ^{13}C- and ^{15}N-isotope labelled guanine residues were analyzed with the use of 2D ^{13}C- and ^{15}N-edited HSQC spectra (Fig. 3). Indeed, this strategy enabled assignment of the imino ^{1}H NMR signals corresponding to the twelve guanines and furthermore demonstrated that they constitute the three G-quartets of L12 G-quadruplex, which represents the minor form in the presence of Na^+ ions. However, the significant overlap of non-exchangeable aromatic NMR signals of guanine residues aggravated

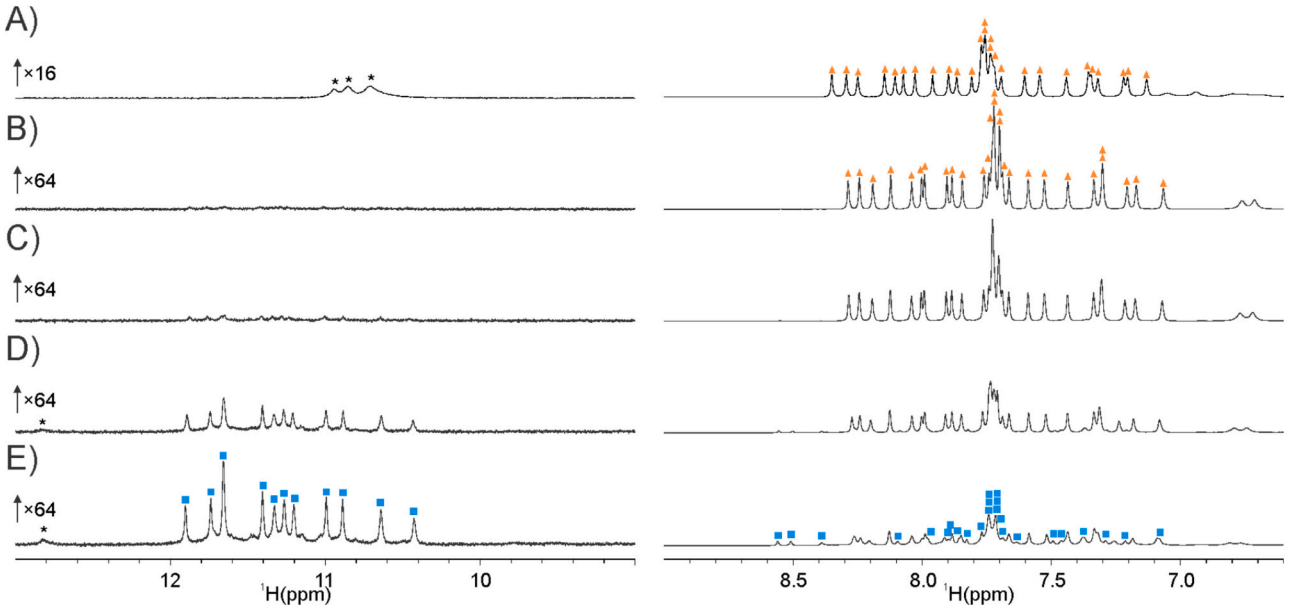

Fig. 2. Imino (left) and aromatic (right) regions of representative ^{1}H NMR spectra of A) desalted L12 in pure water and B-E) L12 after addition of 20 mM NaPi buffer (pH 7.0) and different concentrations of NaCl: B) 0 mM, C) 10 mM, D) 50 mM and E) 100 mM. Vertical scales of the imino with respect to the corresponding aromatic spectral regions are increased as indicated on the left side. Orange triangles and blue squares designate the signals corresponding to single-stranded unstructured oligonucleotide and G-quadruplex, respectively, formed upon addition of Na^+ ions. The imino signals indicated with asterisks were not unambiguously assigned. The spectra were recorded on a 600 MHz NMR spectrometer in 90%/10% $H_2O/^2H_2O$ at 25 °C and A) 0.2 mM or B-E) 1.0 mM oligonucleotide concentration.

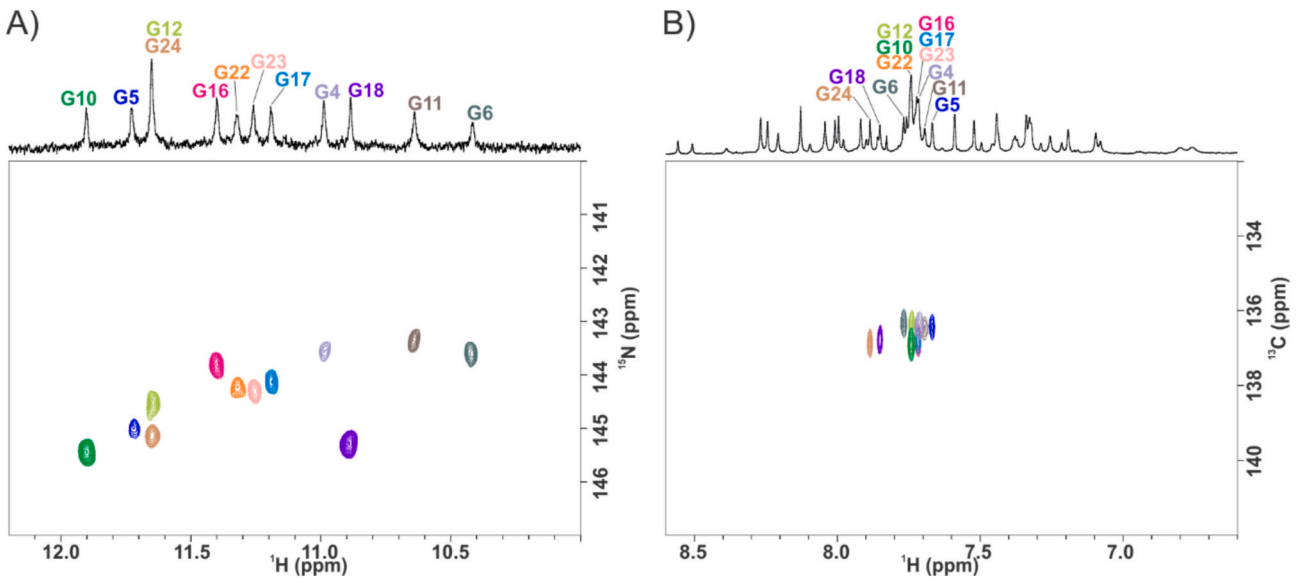

Fig. 3. Stack of A) ^{15}N- and B) ^{13}C-edited 2D HSQC spectra of L12 in the presence of 100 mM NaCl with the corresponding ^{1}H imino and aromatic regions (in panels A and B, respectively) shown on top of the 2D plots. The stacked 2D plots correspond to the spectra acquired on the series of L12 with partially (*ca.* 5%) ^{15}N/^{13}C-labelled single guanine, *i.e.* G4, G5, G6, G10, G11, G12, G16, G17, G18, G22, G23 or G24. The spectra were recorded on a 600 MHz NMR spectrometer in 90%/10% H_2O/$^{2}H_2O$ at 25 °C, 0.2 mM oligonucleotide concentration per strand, 20 mM NaPi buffer (pH 7.0) and 100 mM NaCl.

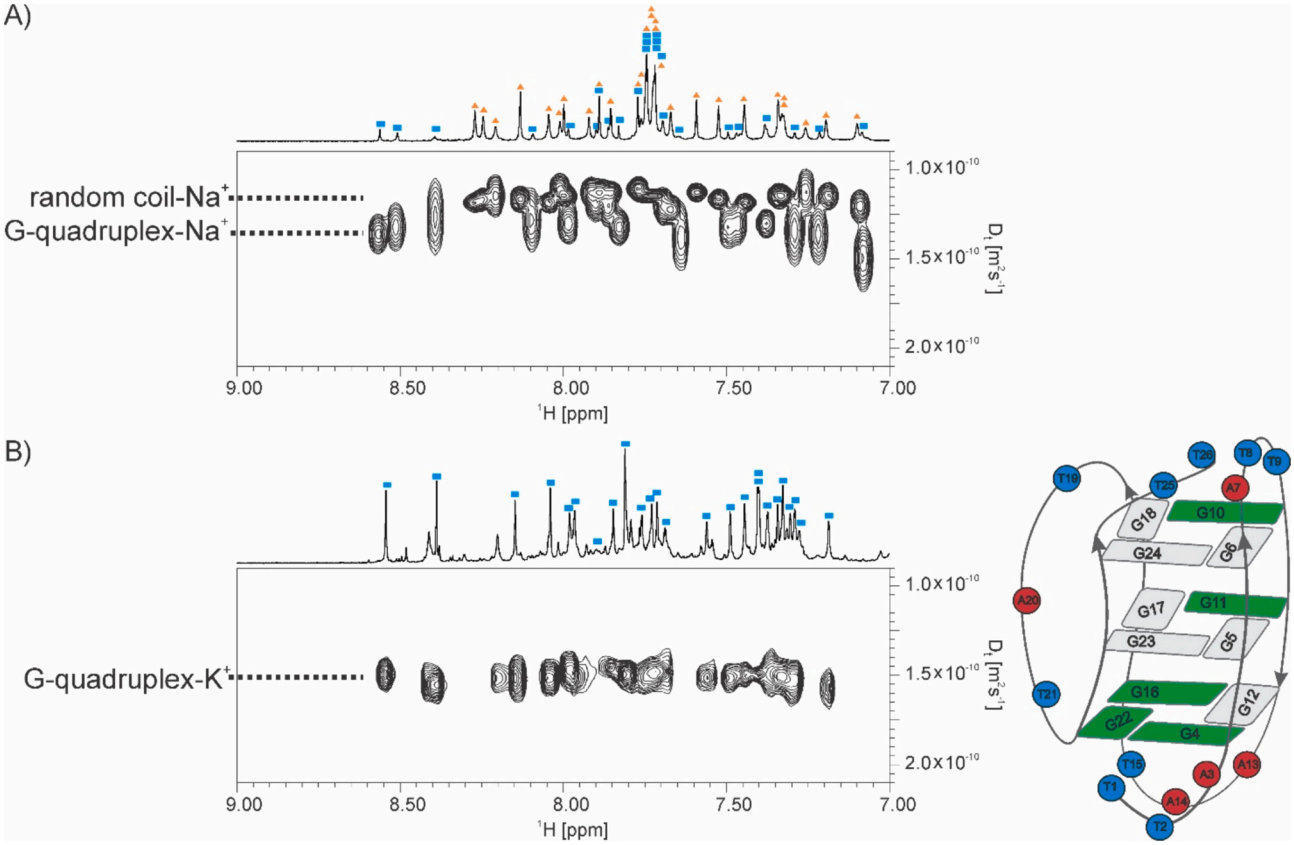

Fig. 4. Aromatic region of 2D DOSY spectra of L12 in the presence of A) Na^+ and B) K^+ ions. The corresponding ^{1}H NMR spectra are shown on the top, whereby orange triangles and blue squares indicate signals for the single-stranded oligonucleotide in random coil and the G-quadruplex, respectively. Schematic representation of the hybrid-2 L12 G-quadruplex is shown on the right side in panel B), with guanines exhibiting *anti* and *syn* glycosidic bond angle dispositions coloured in grey and green, respectively, while the thymine and adenine residues are depicted with blue and red circles, respectively. The lines represent the sugar-phosphate backbone, and the arrows indicate the 5′ → 3′ directionality of the DNA strand throughout the G-quadruplex structure. The spectra were recorded on a 600 MHz NMR spectrometer in 90%/10% H_2O/$^{2}H_2O$ at 25 °C, 1.0 mM oligonucleotide concentration per strand and in A) 20 mM NaPi buffer (pH 7.0) and 100 mM NaCl or B) 20 mM KPi buffer (pH 7.0) and 100 mM KCl.

their complete assignment. Particularly, while the series of ^{13}C-edited HSQC spectra enabled assignment of guanine aromatic signals for the random coil DNA (Fig. 3B), *ca.* 5% ^{13}C-isotopic enrichment proved to be insufficient for resolving signals of the minor and major forms. Specifically, the ^{13}C–^{1}H HSQC cross-peaks for the approximately 4-times less abundant G-quadruplex could not be observed and discriminated from the cross-peaks of the random coil DNA, which arise from *ca.* 1% ^{13}C natural abundance. Detailed NMR-based structural assessment, such as with the use of NOESY analysis, was thus precluded, because of the low amount of the L12 G-quadruplex formed in the presence of exclusively Na^+ ions, as well as of equilibria giving rise to the overlap of NMR signals for the G-quadruplex and random coil species. Notably, however, the presence of imino-imino NOESY cross-peaks, particularly the observed G4H1-G12/G24H1 correlation(s), showed that L12 G-quadruplex adopted either hybrid or antiparallel, but not parallel G-quadruplex folding topology (Fig. S3).

Additionally, it was possible to delineate the different hydrodynamic properties of the species in equilibrium with the use of diffusion ordered spectroscopy (DOSY) (Figs. 4A and S4). In detail, from DOSY analysis the translation diffusion coefficient (D_t) values of 1.2 ($\pm$ 0.1) $\times$ 10^{-10} $m^2 \times s^{-1}$ and 1.3 ($\pm$ 0.1) $\times$ 10^{-10} $m^2 \times s^{-1}$ were obtained for the random coil and G-quadruplex DNA, respectively, consistent with the former corresponding to a loose single-strand, and the latter to a more compact conformation.

In addition to the NMR characterization, L12 was studied in a Na^+-containing buffer also by SE-HPLC and CD. SE-HPLC analysis proved that L12, at 2 μM concentration in 20 mM NaPi buffer (pH 7.0) supplemented with 100 mM NaCl, formed only monomeric species, as inferred by the presence of a single peak in the chromatogram with a retention time typical of L12 unimolecular species [5]. Notably, a single peak was observed for L12 samples even at 20 and 200 μM concentration (Fig. S5A), confirming that the G-quadruplex structure formed in the presence of Na^+ ions was intramolecular, in agreement with the NMR data.

In analogy to the above NMR experiments, a CD-monitored titration of L12 was carried out by adding increasing volumes of the NaPi buffer (pH 7.0) to a L12 solution in pure water, so to obtain a final NaPi concentration of 20 mM, and then increasing amounts of NaCl, so to reach a final concentration of 100 mM. L12 in a salt-free solution at 20 °C appeared as fully unfolded (Fig. S5B, black line). After addition of 20 mM NaPi and even 10 mM NaCl, the CD spectrum remained essentially unaltered (Fig. S5B, red and blue lines, respectively). Further addition of NaCl (from 50 to 100 mM) induced partial folding of L12 into an antiparallel G-quadruplex structure (Fig. S5B, magenta and green lines, respectively), characterized by the typical band at 295 nm [14]. Finally, for L12 in 20 mM NaPi/100 mM NaCl buffer (pH 7.0), obtained at the end of the titration, the thermal denaturation process was followed by recording a CD melting curve, monitoring the CD signal of the main band at 295 nm upon increasing the temperature (Fig. S5C). A melting temperature (T_m) value of 27 °C was found, thus confirming, in agreement with NMR data, the low thermal stability of the L12 G-quadruplex formed in the presence of Na^+ ions.

Additionally, during the CD-melting experiment, CD spectra of the sample were recorded every 5 °C (in Fig. S5D only the spectra at 20, 40 and 70 °C were reported for clarity). At 20 °C, two positive bands were observed, *i.e.* a sharp band at 295 nm and a broad one at 258 nm (Fig. S5D, black line). At 40 °C, the obtained CD profile (Fig. S5D, red line) was very similar to the CD spectra of L12 at low-salt content, *e.g.* in 20 mM NaPi or 20 mM NaPi/10 mM NaCl (Fig. S5B, red and blue lines), essentially attributable to L12 random coil species, since the G-quadruplex structure at this temperature was almost fully denatured. Thus, at 20 °C, the net band at 295 nm can account for the presence of an antiparallel G-quadruplex [14] whereas the second, broader band at 258 nm could result from the overlap of the contribution of the 245 nm band, typical of antiparallel G-quadruplexes, and the 258 nm band of the random coil L12. Thus, CD data confirmed the presence of both folded and unfolded L12 in the Na^+-containing buffer, in full agreement with NMR data.

3.1.2. *Studies of L12 aptamer in K^+-containing buffer*

The ^{1}H NMR spectrum of L12 in 20 mM potassium phosphate (KPi) buffer exhibited several sets of imino signals within the range characteristic of Hoogsteen-hydrogen bonded guanines (Fig. 5A). In detail, besides twelve major imino signals, also twenty resolved minor imino signals were observed between δ ^{1}H 10.6 to 12.1 ppm, consistent with an equilibrium between one major and several minor G-quadruplex structures adopted by L12 in KPi buffer. Upon adding KCl up to 100 mM to L12 in KPi buffer, the imino as well as other ^{1}H NMR spectral signals corresponding to the initially predominant G-quadruplex structures gradually intensified and became better resolved (Fig. 5B-D). Yet, low intensity signals corresponding to minor G-quadruplex species were still observed, with an estimated ratio between 10 and 20% at 100 mM KCl. Notably, the ratio between the major and minor G-quadruplexes was roughly the same even upon further increasing the KCl content to 200 mM, raising the temperature in the range between 5 and 37 °C (Fig. S6) or varying the oligonucleotide concentration from 0.2 to 1.0 mM (Fig. S7). The latter observation is consistent with the G-quadruplexes adopted by L12 upon titration with K^+ ions exhibiting intramolecular topologies.

Series of 2D ^{13}C- and ^{15}N-edited HSQC spectra acquired on site-specifically ^{13}C- and ^{15}N-isotope labelled L12 oligonucleotides enabled assignment of all imino and methyl as well as most of the aromatic and sugar ^{1}H NMR chemical shifts for L12 G-quadruplex formed in aqueous solution comprising K^+ ions (Figs. 6 and S8, Table S1).

Notably, the downfield δ ^{13}C chemical shifts observed for C8 atoms of G4, G10, G11, G16 and G22 indicated that these guanines adopt a *syn* conformation with respect to the glycosidic bond torsion angle (χ), while all the other residues exhibit *anti* conformation [15–19]. This finding was corroborated by complementary NMR-based structural data, including the observed five strong intraresidual H1'-H8 NOESY cross-peaks corresponding to the aforementioned guanine residues (Fig. 7A and S9A). By analyzing intra- and internucleotide NOESY cross-peaks we elucidated the mutual arrangement of guanines in the core as well as of adenine and thymine residues in the loop and overhanging regions of the L12 G-quadruplex formed in the presence of K^+ ions. In detail, G4 → G22 → G16 → G12, G5 → G11 → G17 → G23 and G6 → G10 → G18 → G24 quartets constitute the central part of the L12 G-quadruplex in the presence of K^+ ions. The first three G-tracts, *i.e.* G4-G5-G6, G10-G11-G12 and G16-G17-G18 are linked by two lateral loops (A7-T8-T9 and A13-A14-T15), while the third loop (T19-A20-T21) is of propeller-type. Hence, the orientation of the sugar backbone at the second G-tract is opposite with respect to those of the first and the last two G-tracts, consistent with hybrid-2 G-quadruplex topology.

By using NMR-based structural restraints and simulated annealing approach we calculated the high-resolution structure of L12 G-quadruplex formed in the presence of K^+ ions (Figs. 8, 9 and S10, Table S2).

Inspection of ensemble of the ten lowest energy structures of L12 G-quadruplex shows that the core of the structure is well-defined and comprises three G-quartets, whereby all consecutive guanines are firmly stacked. While partly flexible, the conformation of the 5′-end, *i.e.* T1-T2-A3, and A13-A14-T15 lateral loop appears coupled, with the most unswerving interactions observed between A3 and T15. In detail, all structures within the ensemble exhibit a close positioning of A3 H61 and N1 with respect to T15 O4 and H3, respectively, suggesting a possible formation of reverse Watson-Crick A3:T15 base pair (Fig. 9A). To test this hypothesis, we analyzed 2D ^{15}N-edited HSQC spectra of L12 oligonucleotide with site-specific ^{15}N-isotope labelling at T15, which enabled unambiguous assignment of the broad ^{1}H NMR signal at δ *ca.* 13.5 ppm to the T15 imino proton (Fig. S11A). However, the stable formation of A3:T15 base pair remains tentative, in view that T15 imino proton shows no inter-residual NOE interactions and exhibits fast exchange with bulk water. Furthermore, the A3 and T15 nucleobases in the

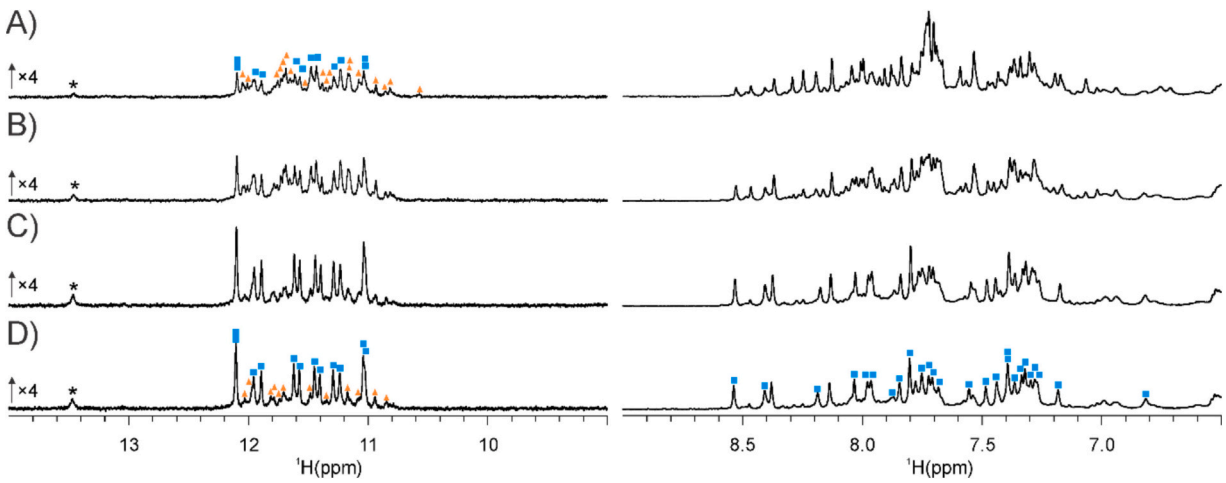

Fig. 5. Imino (left) and aromatic (right) regions of representative ^{1}H NMR spectra of L12 at 20 mM KPi buffer (pH 7.0) and at different concentrations of KCl: A) 0, B) 10, C) 50 and D) 100 mM. Vertical scale of the imino with respect to the corresponding aromatic spectral regions is increased as indicated on the left side. Blue squares are used to indicate signals for imino and aromatic H6/H8 protons corresponding to the major G-quadruplex species at 100 mM KCl. Orange triangles indicate signals corresponding to the minor species. The imino signal at *ca.* δ ^{1}H 13.5 ppm marked with an asterisk corresponds to T15, but was not uniquely assigned to a specific species in the equilibrium. The spectra were recorded on a 600 MHz NMR spectrometer in 90%/10% $H_2O/^2H_2O$ at 25 °C and 0.2 mM oligonucleotide concentration per strand.

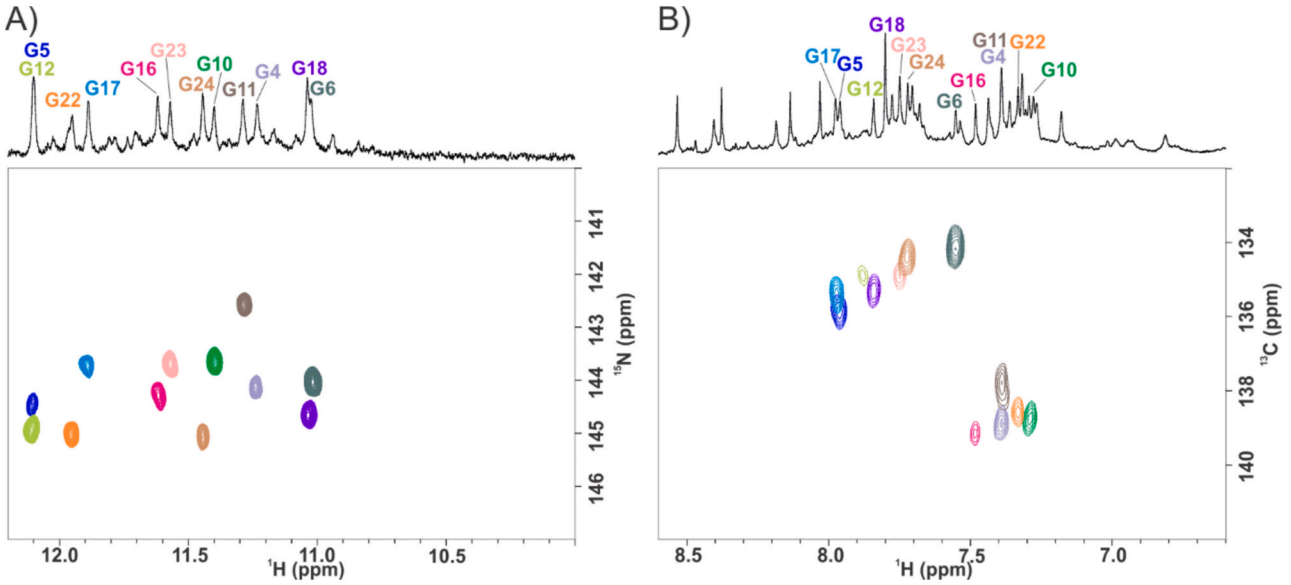

Fig. 6. Stack of A) ^{15}N- and B) ^{13}C-edited 2D HSQC spectra of L12 in the presence of 100 mM KCl with the corresponding ^{1}H imino and aromatic regions (in panels A and B, respectively) shown on top of the 2D plots. The stacked 2D plots correspond to the spectra acquired on the series of L12 with partially (*ca.* 5%) ^{15}N/^{13}C-labelled single guanine, *i.e.* G4, G5, G6, G10, G11, G12, G16, G17, G18, G22, G23 or G24. The spectra were recorded on a 600 MHz NMR spectrometer in 90%/10% $H_2O/^2H_2O$ at 25 °C, 0.2 mM oligonucleotide concentration per strand, 20 mM KPi buffer (pH 7.0) and 100 mM KCl.

calculated ensemble are not strictly coplanar, indicating their interactions, particularly hydrogen-bonding, may be transient or dynamically disordered. Moreover, stacking of T2 over A3 and transient stacking of rather flexible T1 and A14 are observed. These elements expectedly influence the pace of the dynamical interactions of the 5′-end and the nearby lateral loop that are positioned over the G4 → G22 → G16 → G12 quartet, thereby jointly capping the central cation cavity of the structure. Interestingly, one among ten representative structures shows stacking between otherwise flexible T1 and T21. Notably, T21 exhibits a moderate degree of plasticity, but the corresponding nucleobase in most of the structures in the ensemble appears aligned with the plane of A3. In fact, in few structures of the ensemble there are proximities of T21 O4 and A3 H62 as well as of T21 H3 and A3 N7, suggesting potential A3:T21 base pair, which together with the tentative reverse Watson-Crick A3:T15 base pair suggests possible formation of a transient T15:A3:T21 triad. Indeed, T21 seems more flexible than the rest of the corresponding propeller-type loop in which T19 and A20 are well-defined, showing their nucleobases stack. Notably, the interaction of T19 and A20 promotes rather peculiar disposition of T19 methyl groups, which are oriented towards the groove defined by the strands at G16-G17-G18 and G22-G23-G24 segments. G6 → G10 → G18 → G24 quartet is capped with the lateral loop, whereby A7 stacks on G6, while T9 on G18. This disposition of the lateral loop appears further stabilized in several structures of the ensemble, in which stacking of T8 over A7 is observed. The least defined part of the L12 G-quadruplex is the 3′-end overhang, with T25 only transiently stacked over G24 and otherwise together with T26 exhibiting flexible conformation.

Finally, DOSY analysis provided a D_t of 1.5 (± 0.1) × 10^{-10} $m^2 \times s^{-1}$

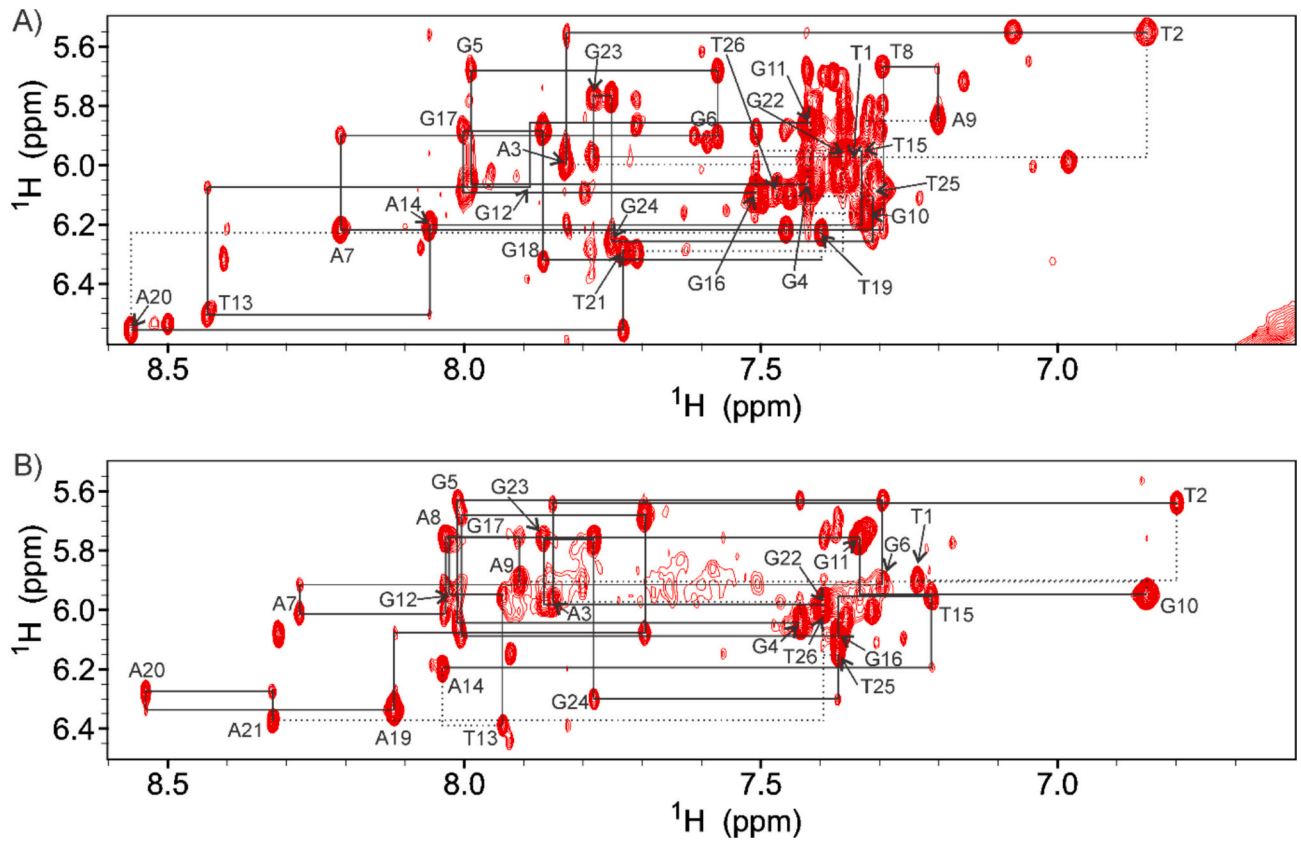

Fig. 7. Anomeric-aromatic region of the 2D NOESY spectrum of A) L12 and B) L41. Residue numbers indicate intraresidual H1'–H6/H8 NOE interactions and the lines the sequential H1′ (i)-H6/H8 (i + 1) correlations. Dotted lines denote weak or absent sequential correlations. The spectra were recorded on an 800 MHz NMR spectrometer in 90%/10% $H_2O/^2H_2O$ at 25 °C, 1.0 mM oligonucleotide concentration per strand, 20 mM KPi buffer (pH 7.0), 100 mM KCl and at τm = A) 120 ms and B) 200 ms.

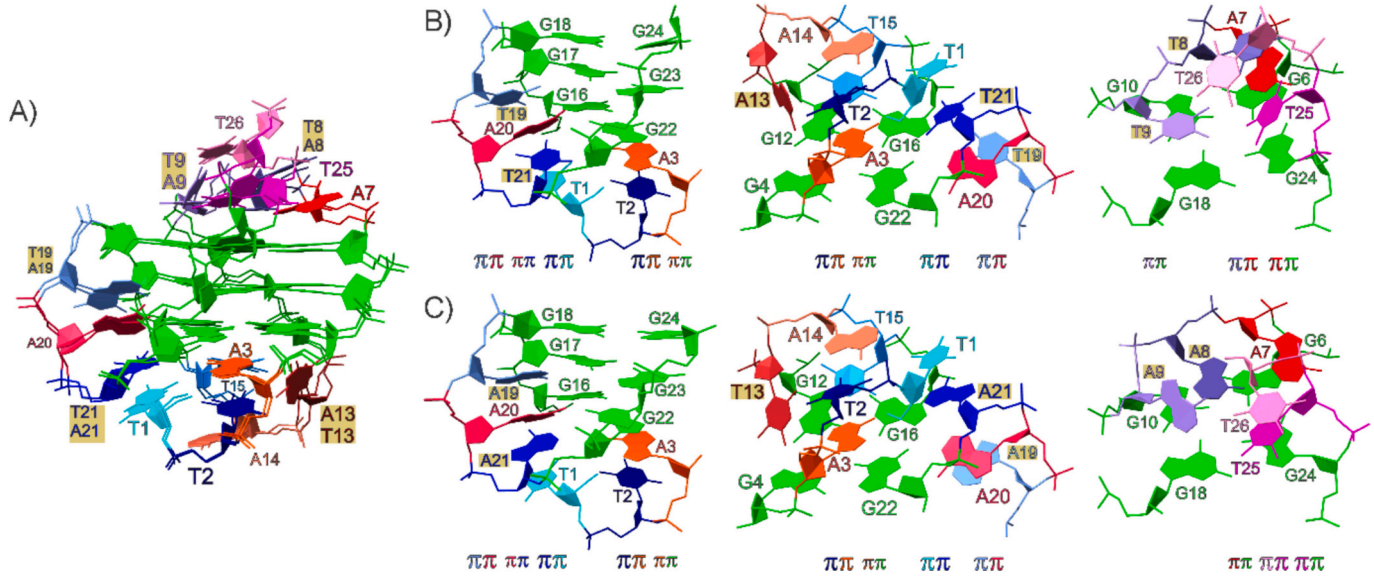

Fig. 8. A) Superposition of the calculated high-resolution solution-state structures of L12 and L41 G-quadruplexes formed in the presence of K^+ ions and details of B) L12 and C) L41 G-quadruplexes. The residue atoms are colour-matched with the residue designations. Hydrogen atoms are not displayed. The successive π symbols indicate stacking interactions between loop, overhanging and guanine residues, with smaller and larger font size used to designate less and more prominent stacking interactions, respectively. Residues that differ in L12 and L41, *i.e.* T8/A8, T9/A9, A13/T13, T19/A19 and T21/A21, are highlighted with a gold background.

for the major hybrid-2 G-quadruplex form of L12 in the presence of K^+ ions (Fig. 4B), further suggesting that the major folding topologies of L12 in Na^+ and K^+ ions are different (antiparallel *vs.* hybrid-2) and/or endowed with different thermodynamic stabilities, with the G-quadruplex formed in the presence of K^+ ions being more compact than the one adopted in Na^+ ions.

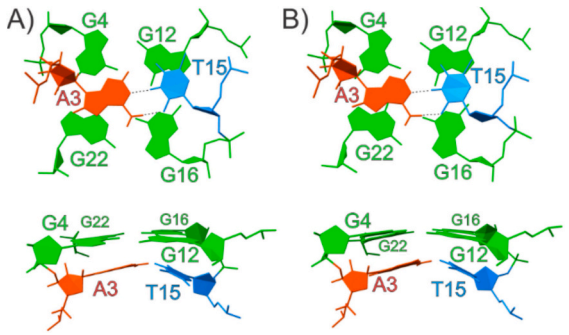

Fig. 9. Top and side views on G4-G22-G16-G12 quartet and the nearby A3 and T15 residues in the lowest energy solution-state structures of A) L12 and B) L41 G-quadruplexes formed in the presence of K^+ ions. Guanines are coloured in green. A3 and T15 are coloured in dark orange and light blue, respectively. A3 H61 and H62, and T15 H3 are the only hydrogen atoms displayed. The dashed lines indicate potential hydrogen bonds.

L12 in the K^+-containing buffer was further characterized by SE-HPLC and CD. The chromatographic profile of L12 at 2 μM concentration in 20 mM KPi buffer (pH 7.0) titrated with up to 100 mM KCl evidenced only one peak, corresponding to the major monomeric NMR-resolved G-quadruplex species of L12 (Fig. S12A). The chromatographic analysis of L12 in this buffer evidenced the presence of a single peak even when the oligonucleotide concentration was increased up to 200 μM (data not shown), confirming, in agreement with NMR data, the formation of an intramolecular G-quadruplex structure also in these conditions. Analogously to the NMR experiments, a CD titration experiment was carried out by adding increasing volumes of the KPi buffer (pH 7.0) to a desalted L12 solution, so to obtain a final KPi concentration of 20 mM, and then adding increasing amounts of KCl, so to reach the final concentration of 100 mM (Fig. S12B, green line). Notably, the addition of K^+ ions induced the formation of a G-quadruplex of hybrid-2 topology, as inferred by the appearance of a band with a maximum at 290 nm and a shoulder at 270 nm [14] even at low K^+ ions concentration, whose intensities increased on increasing the K^+ ions amount (Fig. S12B), in full agreement with NMR data. Consistently with NMR data, further KCl additions up to 200 mM did not produce additional changes to the L12 CD profile (Fig. S12B, grey line). Finally, for L12 in 20 mM KPi/100 mM KCl buffer (pH 7.0) a CD melting curve was recorded by monitoring the CD signal of the main band at 290 nm upon increasing the temperature (Fig. S12C, black line). The obtained T_m value of 55 °C proved the higher thermal stability of the L12 G-quadruplex formed in the presence of K^+ ions compared to the one in Na^+ ions.

Remarkably, on comparing the CD (Fig. S12D) and NMR (Figs. S13D *vs.* S13A) spectra of monomeric L12 in the K^+-containing buffer with the ones in PBS, it emerges that the major fold obtained and resolved by NMR (Fig. 8) in the K^+-rich buffer, *i.e.* a hybrid-2 G-quadruplex, is essentially the same found in PBS. However, lower structuring (Fig. S12D) and lower thermal stability (T_m values of 35 *vs.* 55 °C, Fig. S12C) were evidenced in PBS than in the 20 mM KPi/100 mM KCl buffer (pH 7.0), as expected due to the lower amount of stabilizing K^+ ions.

3.1.3. Studies of L41 aptamer in Na^+- or K^+-containing buffer

The ^{1}H NMR imino region of L41 acquired in absence of salts showed broad signals that were almost at the baseline level, consistent with the absence of a well-defined secondary structure (Fig. S14A). The spectral changes upon titration with K^+ ions were drastic and included appearance of well-resolved imino signals in the spectral region characteristic for Hoogsteen-hydrogen bonded guanines, indicative of formation of G-quartets (Fig. S14B). Moreover, the number of imino ^{1}H NMR signals observed immediately after addition of K^+ ions suggested equilibrium of major and minor G-quadruplexes, whereby the amount of the former increased in the course of time, after 24 h giving *ca.* 90% of the G-quadruplex with three G-quartets (Figs. S14B-C). With the use of 2D NMR spectra, in particular DQF COSY, ^{13}C–^{1}H HSQC and NOESY, most of the ^{1}H NMR signals corresponding to the predominant L41 G-quadruplex were assigned (Figs. 7B and S9B, Table S3). Analysis of NOESY cross-peaks demonstrated that the major L41 G-quadruplex in 20 mM KPi buffer (pH 7.0) and 100 mM KCl exhibited hybrid-2 folding topology, analogously to L12. Interestingly, six strong NOESY cross-peaks corresponding to intraresidual H1'-H8 correlations within G4, G10, G11, G16, G22 and A19 were observed, consistent with their glycosidic bond torsion angle (χ) in *syn* conformation. For all other residues an *anti* disposition was observed.

Noteworthy, ^{1}H NMR-monitored titration of desalted L41 with Na^+ ions at 25 °C (Fig. S15) showed profound changes in aromatic and methyl spectral regions, including broadening of the initial signals as well as appearance of additional broad and poorly resolved signals. Furthermore, addition of Na^+ ions to L41 was coupled also to appearance of imino ^{1}H NMR signals at chemical shift range between δ ^{1}H 10.4 and 11.8 ppm, consistent with formation of G-quadruplex structures. The imino signals, however, were observed almost at the baseline level, which together with the broad signals in other spectral regions suggested that in the presence of Na^+ ions L41 adopts different structures, including a G-quadruplex, with presumably low thermal stabilities.

Calculation of high-resolution L41 G-quadruplex structure formed in the presence of K^+ ions (Figs. 8, 9 and S16) relied on simulated annealing protocol that included 486 distance and 26 torsion angle NMR-based restraints (Table S4). The ensemble of ten representative structures exhibits well converged core, with a pairwise heavy atom RMSD of 0.74 Å. The overall pairwise heavy atom RMSD of 1.66 Å, however, reflects rather loose conformation of several residues, in particular T1 and especially T13. Moreover, five among ten structures exhibit T1 stacked on A21, while otherwise T1 appears flexible. In most of the ensemble structures A21 amino group is pointing towards G16 sugar moiety. Another feature appearing crucial for the stiffness of the A19-A20-A21 propeller-type loop is the stacking of A19 and A20, consistently observed in all structures of the ensemble. While T1 transiently stacks on A21, T2 is well defined and stacked over A3. Furthermore, analysis of the L41 structural ensemble shows that A3 H61 and N1 are consistently positioned in proximity of T15 O4 and H3, respectively. This arrangement is indicative of the potential formation of reverse Watson-Crick A3:T15 base pair (Fig. 9B), which is consistent with the broad imino signal at *ca.* 13.4 ppm assigned to T15 (Fig. S11B). Notably, however, the A3 and T15 nucleobases in the calculated models are not strictly coplanar. This observation, combined with the lack of inter-residual NOE interaction for the T15 imino proton and its fast exchange with the bulk water, demonstrates that the interactions between A3 and T15 are dynamic. This feature of L41 G-quadruplex is analogous to that observed for L12 G-quadruplex. Interestingly, in almost all the structures, A14 amino group is closely positioned to T2 O4' and phosphate groups, consistent with potential hydrogen-bonding. The altogether disposition of the 5'-end T1-T2-A3 and propeller loop A19-A20-A21 appears as a cap over G4→G22→G16→G12 quartet, matching the characteristics observed also for L12 G-quadruplex. Details of the 3'-end and A7-A8-A9 lateral loop that cap the well-defined G6 → G10 → G18 → G24 quartet in L41 G-quadruplexes show some diversity with respect to L12 G-quadruplex. In detail, propensity of A7 to stack over G6 is evident also in L41 G-quadruplex, but to a lesser extent than in L12 G-quadruplex. In the latter, T8 is stacked over A7 in almost all ensemble, while in case of L41 G-quadruplex there seem to be two clusters of structures, whereby A8 either stacks on A7, or orientates away from A7 and stacks on A9. However, the 3′-end of L41 G-quadruplex is well-defined, demonstrating stacking of G24-T25-T26 nucleobases, which is not evident on L12 G-quadruplex.

CD and SE-HPLC data were consistent with the NMR-derived findings. SE-HPLC analysis proved that L41 at 2, 20 and 200 μM

concentration in 20 mM KPi or NaPi buffer (pH 7.0), supplemented with 100 mM KCl or NaCl, respectively, formed only monomeric species (Fig. S17A).

Moreover, in pure water L41 showed a single CD band at 257 nm with a weak and broad minimum at 281 nm, indicative of a low structuration degree in the absence of metal cations (Fig. S17B, black line). Then, addition of 20 mM KPi resulted in well-defined CD spectral changes, producing a new band at *ca.* 295 nm. Upon addition of KCl up to 100 mM the intensity of this band gradually increased and concomitantly its maximum shifted to 290 nm (Fig. S17B). Thus, CD analysis confirmed for L41 the main folding in a G-quadruplex of hybrid conformation in the K^+-containing buffer, with the diagnostic intense positive band at 290 nm and the shoulder at 269 nm. CD melting experiments, monitoring the characteristic band at 290 nm, allowed determining a T_m value of 53 °C for this G-quadruplex structure (Fig. S17C, black line), showing a thermal stability similar to the one of L12 under the same conditions.

In the Na^+-containing buffer the overall stability and degree of structuration of the folded L41 were lower than in the K^+-containing buffer, as in the case of L12, even in the presence of the highest NaCl concentration tested (100 mM), as evidenced by CD melting and CD spectra analysis (Figs. S17C and D, respectively). These findings were in good agreement with NMR data showing that, in the presence of Na^+, L41 adopts different structures, including low amounts of G-quadruplexes, featured by low thermal stabilities, and high amounts of random coil conformations. Indeed, the thermal denaturation of L41 in the Na^+ buffer, on monitoring the CD signals of both the observed bands, *i.e.* the highest one at 259 nm and the very low one at 298 nm, evidenced a sigmoidal transition only for the latter one (blue line, Fig. S17C; T_m of about 29 °C) which may be attributable to a G-quadruplex structure, probably of antiparallel topology. In contrast, the CD signal at 259 nm (generally associated to parallel G-quadruplex topologies) monitored on increasing the temperature from 10 to 80 °C produced only a drift curve (red line, Fig. S17C), proving that it is probably correlated to the random coil form of L41. Indeed, the CD spectra of L41 in 100 mM lithium chloride buffer (a high ionic strength medium that disfavours G-quadruplex formation) showed a high-intensity band at 260 nm almost overlapping the one of the aptamer at the same concentration in the sodium-only buffer (*cfr.* red and green lines of Fig. S17E). Furthermore, the CD spectra of L41 in the sodium-only buffer at 80 °C confirmed that the stacking interactions of the random-coil conformation of this aptamer were completely disrupted at this temperature (Fig. S17F). By comparison of CD (Fig. S17G) and NMR (Figs. S18D *vs.* S18A) spectra of the monomeric L41 in the K^+-containing buffer with the ones in PBS, it emerges that the major folding prevalent in only K^+ buffer, resolved by NMR, *i.e.* a hybrid-2 G-quadruplex, is also the one present in PBS which coexists with a random coil conformation.

Finally, comparison of the CD spectra of the monomeric L12 and L41 in PBS (Fig. 10A) shows that the amount of structuring in a hybrid-2 G-quadruplex topology, characterized by the band with maximum at 290 nm, should be higher for L12 than for L41, which in turn is featured by a higher amount of random coil oligonucleotide, featured by the band with maximum at *ca.* 260 nm (Fig. S17E). Thus, it can be hypothesized that the presence of two AAA loops (all-purine three base loops) in the examined L41 sequence, not present in L12, stabilizes the random coil conformations, in turn impairing the G-quadruplex folding of this specific oligonucleotide sequence, unless high K^+ concentrations are present, and in this case monomeric G-quadruplexes similar in structure (Figs. 8 and 10B) and thermal stability (Figs. S12C and S17C, black lines) are formed for the two oligonucleotides.

3.2. CD- and BLI-binding studies on the interaction of L12 and L41 aptamers with HMGB1

CD-monitored binding experiments were performed to investigate the interaction of L12 and L41 in monomeric form with HMGB1 in PBS buffer. In detail, a cuvette characterized by two separated chambers, which allows first recording the *sum* spectrum of the oligonucleotide and protein solutions, kept apart in the two chambers, and then the *mix* spectrum, obtained after mixing them, was used. If the analyzed samples do not interact, the *sum* and *mix* spectra are superimposable, otherwise the spectrum obtained after mixing the two solutions differs from the *sum* spectrum. Here, the *mix* spectra of both L12 and L41 (Fig. 11, red lines) were significantly different from the *sum* spectra (Fig. 11, blue lines), thus confirming the interaction between each oligonucleotide and the protein. The major differences between the *sum* and *mix* spectra were observed in the 200–230 nm region, while no changes were detected in the 230–320 nm region (Fig. 11), where it is the DNA to mainly contribute to the CD signal. This finding suggests that no major rearrangement of the L12/L41 G-quadruplex core is detected upon aptamer/protein complexes formation, while more relevant effects were observed for HMGB1, in line with previous studies on HMGB1-DNA interactions [2,5,20–23].

The interaction of L12 and L41 monomers with HMGB1 in PBS buffer was also studied by BLI [13], so to obtain information on the binding affinity of the aptamers towards the protein. The aptamers, in form of their 5′-biotinylated derivatives, were immobilized on streptavidin-coated sensors and incubated with HMGB1 at different concentrations. The 1:1 model was used for the global curve fitting of the experimental data [13] (Fig. S19). K_D values of 220 ± 10 nM and 663 ± 13 nM were obtained for L12 and L41, respectively. These data indicated that, when treated with either L12 or L41 in monomeric form, HMGB1 preferentially bound L12, essentially structured in hybrid-2 G-quadruplex in PBS buffer, and recognized with only a 3-fold lower affinity L41, mainly in a

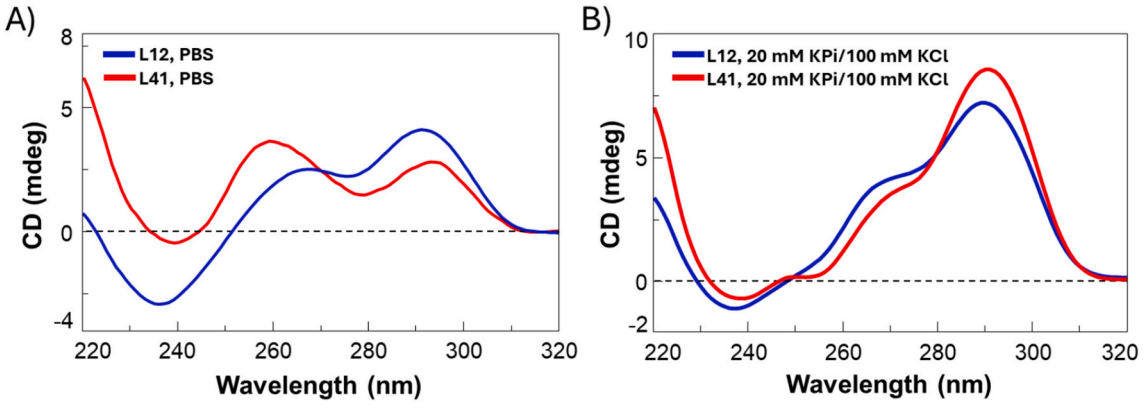

Fig. 10. Representative overlapped CD spectra of L12 (blue lines) and L41 (red lines) monomers at 20 °C, 2 μM DNA concentration in A) PBS and B) 20 mM KPi buffer (pH 7.0), 100 mM KCl.

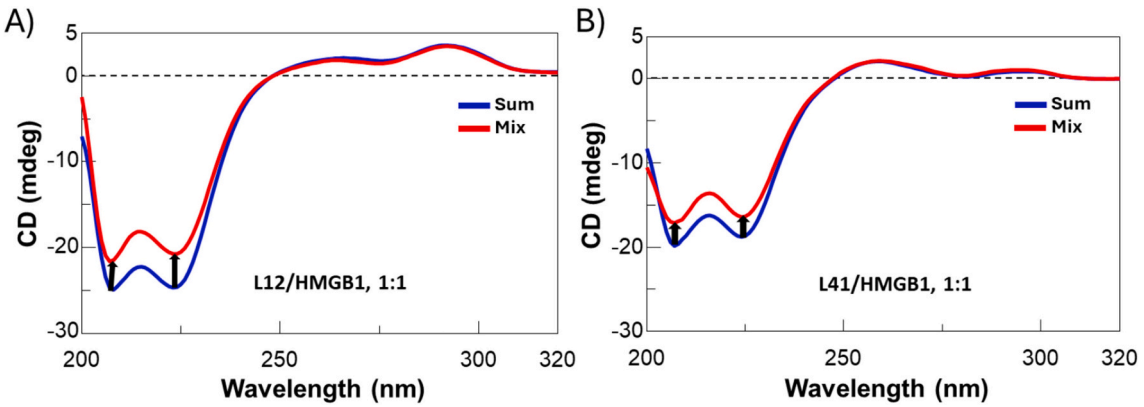

Fig. 11. Representative overlapped *sum* (blue lines) and *mix* (red lines) spectra obtained for the CD-binding experiments of A) L12 and B) L41 with HMGB1. CD spectra were recorded at 20 °C, 2 μM DNA or protein concentration (1:1 DNA/protein ratio) and in PBS buffer.

random-coil and only to a lower extent folded in a hybrid-2 G-quadruplex conformation.

3.3. In vitro cell migration assay

Finally, to test the ability of L12 and L41 monomers to interfere with HMGB1-induced cell migration, a Boyden chamber assay was performed (Fig. 12). In detail, A549 non-small-cell lung cancer (NSCLC) cells – naturally expressing and releasing high levels of HMGB1 and for which a key role of the protein in the self-regulation of cell migration is reported [24,25] – were treated with each aptamer at 100 nM concentration for 24 h. HMGB1-induced cell migration was monitored by using 10% Fetal Bovine Serum (FBS) as chemoattractant stimulus. A scrambled oligonucleotide with the sequence 5′-d(AAG-TGT-GTG-TGT-GTG-TGT-GTG-TGA-AG)-3′ (scr), featured by the same number of guanines as L12 and L41 but unable to form G-quadruplex structures, was used as negative control. Notably, both L12 and L41 hampered HMGB1-induced cell migration, whereas no effect was observed upon treatment with the scr control oligonucleotide (Fig. 12). A stronger inhibition of cell migration was detected for L12 compared to L41 (Fig. 12), in agreement with the higher affinity to HMGB1 found for L12 compared to L41, as determined by BLI analysis.

4. Conclusions

Stimulated by the stringent need to discover novel targeted treatments for still intractable tumours and inflammation-related pathologies, we focused our interest on oligonucleotide aptamers able to specifically recognize the protein HMGB1, which is crucially involved in the pathogenesis of these diseases [1,7,9,26]. Recently, some of us selected a set of G-quadruplex-forming aptamers able to bind HMGB1 and inhibit its extracellular pathological activity, proving that those named L12 and L41 were the most effective ones in terms of affinity and activity towards the protein, as well as enzymatic resistance in serum [4]. These aptamers shared the common feature of forming both monomeric and dimeric/higher-order G-quadruplex structures in PBS, a buffer mimicking the extracellular environment where HMGB1 exerts its pathogenic activity.

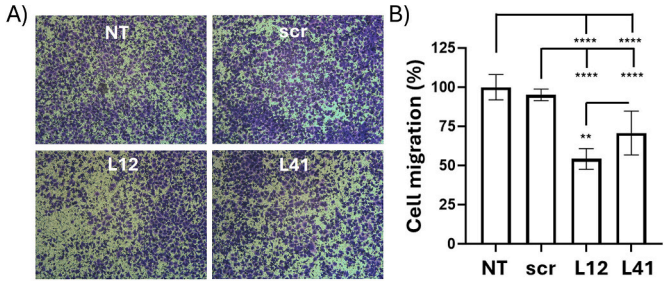

Fig. 12. Migration assay on human A549 lung cancer cells. Not-treated (NT) cells and cells treated for 24 h with 100 nM scrambled oligonucleotide (scr, negative control), monomeric L12 or L41 were allowed migrating for 24 h using 10% FBS as chemoattractant. Migrated cells were stained with 1% Crystal Violet. A) Representative pictures of the migrated cells. Magnification: 10×. B) Migration was quantified by eluting Crystal Violet expressing the absorbance values as % with respect to not-treated cells. Data are presented as mean ± SD from three independent experiments. Statistical analysis was performed by one-way ANOVA with multiple comparisons ($n = 3$): ****, $p < 0.0001$; **, $p < 0.01$.

With the aim of elucidating the peculiar conformational behavior of L12 and L41 in PBS, we have here undertaken an in-depth NMR analysis of these aptamers, complemented by SE-HPLC and CD data. NMR-derived structures were obtained for the monomeric forms of L12 and L41 in K^+-rich solutions. Both aptamers proved to form G-quadruplex structures of hybrid-2 topology with similar features, overall suggesting that the key DNA/protein interfaces are analogous in the protein recognition for both aptamers. However, some differences between the G-quadruplex structures formed by L12 and L41 were found at the 3′-end and the lateral loop capping their 3′-end G-quartet.

Notably, comparing the NMR and CD data obtained in K^+-rich solutions and PBS, we proved that the NMR-solved structures are essentially the same as the prevalent G-quadruplex folds that can be found in a simulated extracellular environment for L12 and L41 in their monomeric forms, respectively, thus allowing us to assume that these G-quadruplex structures may also represent the relevant folds in the actual binding events with the protein under physiological conditions.

Remarkably, L12 in PBS showed a more marked G-quadruplex structuring than L41, for which, in turn, the random coil species was prevailing. This result might be explained on the basis of the higher purine *vs.* pyrimidines content in L41 oligonucleotide sequence than L12 (*i.e.* 20:6 *vs.* 17:9, or, considering only the loops, 7:3 *vs.* 4:5) and also the presence in L41 sequence of two loops with three consecutive adenines accounting for two tracts of 9 sequential purines (TTA-GGG-AAA-GGG-TAT-GGG-AAA-GGG-TT) which in PBS (a buffer with low K^+ concentration) could shift the equilibrium favouring more the random coil species (probably stabilized by stacking of adjacent purines specifically found in L41) rather than the G-quadruplex structures. These differences in the position of the equilibrium G-quadruplex *vs.* random coil are however not observed when high K^+ concentrations are reached, which shift the equilibrium towards quite similar G-quadruplex structures for both the sequences.

L12 and L41 monomers were further analyzed in their interaction with HMGB1 by CD and BLI techniques and finally tested for their anti-HMGB1 activity by *in vitro* assays. Notably, CD analysis proved that, upon aptamer/protein 1:1 complex formation, major structural

rearrangements occurred only for HMGB1, and not for L12 or L41, thus further validating the interaction of these aptamers with the protein and, indirectly, their NMR-derived G-quadruplex structures as the ones recognized by the protein. Interestingly, a net preference of HMGB1 for L12 ($K_D = 220 \pm 10$ nM) over L41 ($K_D = 663 \pm 13$ nM) was observed by BLI analysis. This well matches with the higher anti-HMGB1 activity of the L12 aptamer observed in the Boyden chamber assay, in which a stronger inhibition of cell migration was found upon treatment of A549 NSCLC cells with L12 aptamer compared to L41.

Overall, our studies suggested that HMGB1 preferentially recognizes L12 monomer over L41 monomer in the PBS buffer, probably due to the higher amount of hybrid-2 G-quadruplex structures formed by L12 in these conditions. However, we cannot exclude that the different affinities found for these aptamers towards HMGB1 can be also related to differences in the orientation adopted by the 3′-end and lateral loop residues within the formed hybrid-2 G-quadruplexes, which appeared better stacked on the G-quadruplex core and thus less dynamic in L41 than L12 thus somehow precluding some potential interactions with the protein in the case of L41.

The results presented here revealed the conformational details of the main monomeric G-quadruplex structures of L12 and L41, recently discovered as potential candidate drugs against the HMGB1 protein. Considering the important role of HMGB1 in several pathologies, the here solved NMR structures of these specific targeting agents increase the knowledge of the conformational behavior of inhibitors of this protein and provide a deep understanding at a molecular level of which can be their active conformations. All these novel structural findings will be crucial to direct the rational design of optimized L12/L41 analogues, aimed at obtaining even more effective and selective HMGB1 inhibitors.

CRediT authorship contribution statement

Marko Trajkovski: Writing – review & editing, Writing – original draft, Visualization, Validation, Supervision, Methodology, Investigation, Data curation, Conceptualization. **Chiara Platella:** Writing – review & editing, Writing – original draft, Validation, Supervision, Methodology, Investigation, Data curation, Conceptualization. **Domenica Musumeci:** Writing – review & editing, Writing – original draft, Validation, Supervision, Methodology, Investigation, Funding acquisition, Data curation, Conceptualization. **Ettore Napolitano:** Writing – review & editing, Writing – original draft, Validation, Methodology, Investigation, Data curation, Conceptualization. **Carla Lucia Esposito:** Writing – review & editing, Writing – original draft, Validation, Methodology, Investigation, Data curation, Conceptualization. **Silvia Catuogno:** Writing – review & editing, Writing – original draft, Methodology, Investigation, Data curation. **Janez Plavec:** Writing – review & editing, Writing – original draft, Validation, Supervision, Resources, Methodology, Funding acquisition, Data curation, Conceptualization. **Daniela Montesarchio:** Writing – review & editing, Writing – original draft, Supervision, Resources, Methodology, Funding acquisition, Data curation, Conceptualization.

Funding

The research received funds from: i) Slovenian Research and Innovation Agency [ARIS, grants P1-0242 and J1-60019] and the GIGA NMR project co-financed by the Republic of Slovenia, the Ministry of Higher Education, Science and Innovation, and the European Union under the European Regional Development Fund – P.I. Janez Plavec; ii) the European Union - NextGeneration EU, National Recovery and Resilience Plan (PNRR), Project CN00000041 “National Center for Gene Therapy and Drugs based on RNA Technology”: iii) Fondazione AIRC under IG2020—ID. 25046 — P.I. Montesarchio Daniela; AIRC SIS—ID. 28703 P.I. Esposito Carla Lucia; AIRC—ID. 29052 P.I. Catuogno Silvia; and iv) Federico II University, FRA2022 project (CUP: E65F22000050001) – P.I. Musumeci Domenica.

Declaration of competing interest

The authors declare that they have no known competing financial interests or personal relationships that could have appeared to influence the work reported in this paper.

Acknowledgements

The authors acknowledge the CERIC-ERIC consortium for access to NMR facilities.

Appendix A. Supplementary data

Supplementary data to this article can be found online at https://doi.org/10.1016/j.ijbiomac.2026.151585.

Data availability

L12 NMR structure: PDB ID 9TNR, BMRB ID 35028. L41 NMR structure: PDB ID 9TNQ, BMRB ID 35027.

References

[1] C.K. Voong, J.A. Goodrich, J.F. Kugel, Interactions of HMGB proteins with the genome and the impact on disease, Biomolecules 11 (2021) 1451, https://doi.org/10.3390/biom11101451.
[2] D. Musumeci, E.M. Bucci, G.N. Roviello, R. Sapio, M. Valente, M. Moccia, M. E. Bianchi, C. Pedone, DNA-based strategies for blocking HMGB1 cytokine activity: design, synthesis and preliminary in vitro/in vivo assays of DNA and DNA-like duplexes, Mol. BioSyst. 7 (2011) 1742–1752, https://doi.org/10.1039/c1mb05009e.
[3] D. Musumeci, G.N. Roviello, D. Montesarchio, R. Sapio, M. Valente, V. Anrò, E. M. Bucci, Hairpin ODN-based ligands as potential inhibitors of HMGB1 cytokine activity, RSC Adv. 3 (2013) 12176–12184, https://doi.org/10.1039/c3ra41915k.
[4] E. Napolitano, A. Criscuolo, C. Riccardi, C.L. Esposito, S. Catuogno, G. Coppola, G. N. Roviello, D. Montesarchio, D. Musumeci, Directing in vitro selection towards G-quadruplex-forming aptamers to inhibit HMGB1 pathological activity, Angew. Chem. Int. Ed. 63 (2024) e202319828, https://doi.org/10.1002/anie.202319828.
[5] E. Napolitano, A. Criscuolo, C. Riccardi, C. Platella, R. Gaglione, A. Arciello, D. Musumeci, D. Montesarchio, When annealing is detrimental: the case of HMGB1-targeting G-quadruplex aptamers, Int. J. Biol. Macromol. 283 (2024) 137148, https://doi.org/10.1016/j.ijbiomac.2024.137148.
[6] R. Chen, R. Kang, D. Tang, The mechanism of HMGB1 secretion and release, Exp. Mol. Med. 54 (2022) 91–102, https://doi.org/10.1038/s12276-022-00736-w.
[7] J. Mo, J. Hu, X. Cheng, The role of high mobility group box 1 in neuroinflammatory related diseases, Biomed. Pharmacother. 161 (2023) 114541, https://doi.org/10.1016/j.biopha.2023.114541.
[8] D. Musumeci, G.N. Roviello, D. Montesarchio, An overview on HMGB1 inhibitors as potential therapeutic agents in HMGB1-related pathologies, Pharmacol. Ther. 141 (2014) 347–357, https://doi.org/10.1016/j.pharmthera.2013.11.001.
[9] S. Yuan, Z. Liu, Z. Xu, J. Liu, J. Zhang, High mobility group box 1 (HMGB1): a pivotal regulator of hematopoietic malignancies, J. Hematol. Oncol. 13 (2020) 1186, https://doi.org/10.1186/s13045-020-00920-3.
[10] W. Lee, M. Tonelli, J.L. Markley, NMRFAM-SPARKY: enhanced software for biomolecular NMR spectroscopy, Bioinformatics 31 (2015) 1325–1327, https://doi.org/10.1093/bioinformatics/btu830.
[11] D.A. Case, H.M. Aktulga, K. Belfon, I.Y. Ben-Shalom, J.T. Berryman, S.R. Brozell, et al., Amber 2022, University of California, San Francisco, 2022.
[12] X.J. Lu, W.K. Olson, 3DNA: a software package for the analysis, rebuilding and visualization of three-dimensional nucleic acid structures, Nucleic Acids Res. 31 (2003) 5108–5121, https://doi.org/10.1093/nar/gkg680.
[13] J.K. Barrows, M.W. Van Dyke, Biolayer interferometry for DNA-protein interactions, PLoS One 17 (2022) e0263322, https://doi.org/10.1371/journal.pone.0263322.
[14] Y. Luo, A. Granzhan, J. Marquevielle, A. Cucchiarini, L. Lacroix, S. Amrane, D. Verga, J.L. Mergny, Guidelines for G-quadruplexes: I. In vitro characterization, Biochimie 214 (2023) 5–23, https://doi.org/10.1016/j.biochi.2022.12.019.
[15] L. Haase, J. Dickerhoff, K. Weisz, Sugar puckering drives G-quadruplex refolding: implications for V-shaped loops, Chem. Eur. J. 26 (2020) 524–533, https://doi.org/10.1002/chem.201904044.
[16] Y.M. Vianney, N. Schröder, J. Jana, G. Chojetzki, K. Weisz, Showcasing different G-quadruplex folds of a G-rich sequence: between rule-based prediction and butterfly effect, J. Am. Chem. Soc. 145 (2023) 22194–22205, https://doi.org/10.1021/jacs.3c08336.
[17] M. Juribašić Kulcsár, V. Gabelica, J. Plavec, Solution-state structure of a long-loop G-quadruplex formed within promoters of plasmodium falciparum B var genes, Chem. Eur. J. 30 (2024) e202401190, https://doi.org/10.1002/chem.202401190.

[18] M. Trajkovski, A. Pastore, J. Plavec, Dimeric structures of DNA ATTTC repeats promoted by divalent cations, Nucleic Acids Res. 52 (2024) 1591–1601, https://doi.org/10.1093/nar/gkae052.
[19] N. Medved, M. Cevec, U. Javornik, J. Lah, S. Hadži, J. Plavec, Beyond structure: methylation fine-tunes stability and folding kinetics of bcl2Mid G-quadruplex, Angew. Chem. Int. Ed. 64 (2025) e202507544, https://doi.org/10.1002/anie.202507544.
[20] D. Musumeci, G.N. Roviello, M. Moccia, C. Pedone, E.M. Bucci, R. Sapio, M. Valente, S. Fumero, Bent oligonucleotide duplexes as HMGB1 inhibitors: a comparative study, Nucleosides Nucleotides Nucleic Acids 26 (2007) 1447–1450, https://doi.org/10.1080/15257770701542330.
[21] J. Amato, T.W. Madanayake, N. Iaccarino, E. Novellino, A. Randazzo, L.H. Hurley, B. Pagano, HMGB1 binds to the KRAS promoter G-quadruplex: a new player in oncogene transcriptional regulation? Chem. Commun. 54 (2018) 9442–9445, https://doi.org/10.1039/c8cc03614d.
[22] J. Amato, L. Cerofolini, D. Brancaccio, S. Giuntini, N. Iaccarino, P. Zizza, S. Iachettini, A. Biroccio, E. Novellino, A. Rosato, M. Fragai, C. Luchinat, A. Randazzo, B. Pagano, Insights into telomeric G-quadruplex DNA recognition by HMGB1 protein, Nucleic Acids Res. 47 (2019) 9950–9966, https://doi.org/10.1093/nar/gkz727.
[23] A. Criscuolo, E. Napolitano, C. Riccardi, R. Gaglione, E. Piccolo, A. Arciello, D. Musumeci, D. Montesarchio, Covalently linked dimers of a G-quadruplex-forming aptamer as HMGB1 inhibitors, Int. J. Biol. Macromol. 332 (2025) 148479, https://doi.org/10.1016/j.ijbiomac.2025.148479.
[24] X.H. Wang, S.Y. Zhang, M. Shi, X.P. Xu, HMGB1 promotes the proliferation and metastasis of lung cancer by activating the Wnt/β-catenin pathway, Technol. Cancer Res. Treat. 19 (2020) 1–8, https://doi.org/10.1177/1533033820948054.
[25] Y. Ma, Q. Feng, B. Han, R. Yu, Z. Jin, Elevated HMGB1 promotes the malignant progression and contributes to cisplatin resistance of non-small cell lung cancer, Hereditas 160 (2023) 33, https://doi.org/10.1186/s41065-023-00294-9.
[26] E. Napolitano, A. Criscuolo, C. Riccardi, C. Platella, D. Musumeci, D. Montesarchio, G-Quadruplex-forming aptamers as selective inhibitors of HMGB1 protein: a journey from design to their functional validation, Croat. Chem. Acta 98 (2025) 67–78, https://doi.org/10.5562/cca4189.